Ultrasonography-Derived Elasticity Estimation of Live Porcine Oral Mucosa

Hsi-Chien Yu, DDS, Oliver D. Kripfgans, PhD, Amanda B. Rodriguez, DDS, Ankita Samal, BDS, Carole Quesada, BS, Liana P. Webber, DDS, MS, John P. Mazzocco, DDS, I-Ching Wang, DDS, MS, Jaeman Woo, DMD, MSD, Hsun-Liang Chan, DDS, MS

Received June 1, 2023, from the Department of Radiology, School of Medicine, University of Michigan, Ann Arbor, MI, USA (H.-C.Y., O.D.K., A.S., C.Q.); Department of Oral and Maxillofacial Surgery, Chi Mei Medical Center, Tainan, Taiwan (H.-C.Y.); Department of Periodontics and Oral Medicine, School of Dentistry, University of Michigan, Ann Arbor, MI, USA (A.B.R., L.P.W., J.P.M., H.-L.C.); Department of Periodontics, College of Dentistry and Dental Clinics, University of Iowa, Iowa City, IA, USA (I-Ching.W.); and Department of Dentistry, College of Medicine and Graduate School of Medicine, Jeju National University, Jeju, Republic of Korea (J.W.). Manuscript accepted for publication September 26, 2023.

National Institutes of Health (NIH) Grant (1-R21-DE-029005): Quantitative Estimation of Periodontal Inflammation and Tissue Destruction with High-Resolution Ultrasound-Based Imaging.

Address correspondence to Oliver D. Kripfgans, DDS, MS, Department of Radiology, Medical Science Building I, Room 6410, 1301 Catherine Street, Ann Arbor, MI 48109-2026, USA.

E-mail: oliver.kripfgans@umich.edu

Abbreviations

AM, alveolar mucosa; DIS, distal; G, gingiva; LSG, longitudinal strain gingiva; LSM, longitudinal strain mucosa; MES, mesial; MID, mid-facial; PM3, premolar 3; ROI, region of interest; TSG, tensile strain gingiva; TSG1, tensile strain gingiva at surface; TSG2, tensile strain gingiva, 500 μm below surface; TSG3, tensile strain gingiva, 1000 μm below surface; TSM, tensilestrain mucosa; TSM1, tensilestrain gingiva at surface; TSM2, tensilestrain gingiva, 500 μm below surface; TSM3, tensilestrain gingiva, 1000 μm below surface

doi:10.1002/jum.16352

Objectives—To investigate the biomechanical properties of porcine oral tissues with in vivo ultrasonography and to compare the difference between oral alveolar mucosa and gingival tissue concerning compressional and tensile mechanical strain.

Materials and Methods—Sinclair minipigs (6 females and 4 males, 6 to 18 months of age) were anesthetized for ultrasonography. In vivo high-frequency tissue harmonic ultrasound (12/24 MHz) cine-loops were obtained while inducing mechanical tissue stress (0 to 1 N). Post-processing strain analysis was performed in a cardiac speckle tracking software (EchoInsight®). Region of interest (ROI) was placed for gingival and alveolar mucosa tissues for longitudinal (compressional) and tensile strain analyses. A calibrated gel pad was employed to determine the absolute force (pressure) for the measured tissue strain response function. The resulting elasticity data was statistically analyzed using custom Matlab scripts.

Results—In total, 38 sonography cine-loops around the third premolars were included in the investigation. The longitudinal strain of alveolar mucosa ε^L_{AM} was found to be significantly ($P < .05$) larger than that of gingiva ε^L_G. Across the measured force range, $\varepsilon^L_{AM} \sim 1.7 \times \varepsilon^L_G$. Significant differences between alveolar mucosa and gingiva tissues were found for all forces. The tensile strain of the alveolar mucosa ε^T_{AM} was found to be $\sim 2 \times \varepsilon^T_G$ (on the epithelial surface of the gingiva). Both were statistically significantly different for forces exceeding ~0.08 N. At depth, that is, 500 and 1000 μm below the epithelial surface, the gingiva was found to have less ability to stretch contrary to the alveolar mucosa. Gingival tissue at 500 μm depth has significantly less tensile strain than at its surface and more than at 1000 μm depth. In contrast, the tensile strain of alveolar mucosa is largely independent of depth.

Conclusion—Ultrasonography can reveal significant differences in oral alveolar mucosal and gingival elastic properties, such as compressional and tensile strain. Under minute forces equivalent to 10 to 40 g, these differences can be observed. As dental ultrasound is a chairside, and noninvasive modality, obtaining real-time images might soon find clinical utility as a new diagnostic tool for the objective and quantitative assessment of periodontal and peri-implant soft tissues in clinical and research realms. As ultrasound is a safe modality with no known bioeffects, longitudinal monitoring of areas of concern would be particularly attractive.

Key Words—elasticity; oral mucosa; periodontitis; periodontium; speckle tracking; strain

© 2023 American Institute of Ultrasound in Medicine.

Oral mucosa has unique biological structures and biomechanical properties, therefore acting distinctively in physiological or pathological events.[1] It is broadly classified based on its attachment mode to the underlying structure into the nonattached lining alveolar mucosa (AM) and the attached mucosa, that is, gingiva (G). Alveolar mucosa, forming an anatomical transition from the gingiva to the buccal mucosa, has nonkeratinized stratified squamous epithelium. Additionally, its submucosal layer is rich in elastic fibers and is separated from the underlying bone by muscle fibers, which makes it soft, movable, and flexible. Contrarily, the gingiva does provide a protective function for the tooth and alveolar bone. Due to its stratified squamous epithelium and dense collagenous connective tissue layer, it forms a tense connection with the periosteum. The gingiva is filled with keratin filaments and more condensed alignment epithelial cells. Therefore, the gingiva is believed to withstand injuries to the tooth and periodontium from excessive masticatory forces, mechanical as well as chemical irritation, and bacterial invasion.[2,3]

The biomechanical properties of oral mucosal tissue have been studied using preclinical animal or human cadaverous tissues for understanding oral tissue responses to mastication, speaking, oral parafunction, and dental prostheses.[4–6] In addition, the biomechanical behavior and biological reaction of the oral mucosa have been studied to understand wound healing. For example, a residual tension of as small as 0.5 N in soft tissue flaps after oral regenerative procedures can transduce and affect fibroblasts negatively, potentially resulting in wound edge necrosis and dehiscence. Unfortunately, tissue features may change after processing for ex vivo studies, therefore making a direct extrapolation to live tissue behaviors is very difficult, if not impossible.[4] A methodology to evaluate the biomechanical properties of living human oral tissues is deemed desirable and much needed.[7]

Ultrasonography is a noninvasive and safe imaging method that has been used in the medical field since the middle of the last century.[8] Using different transmit frequencies and imaging modes, ultrasonography can provide information related to anatomic tissue structures, blood flow, tissue elasticity, and more. Previously, due to the space limitation of the oral cavity and the uneven surface of oral anatomy, finding a suitable ultrasound probe for intraoral usage was a challenge. Thanks to technological advances, a high-frequency transducer with a small ergonometric housing was designed for intraoral usage, allowing for the scanning of intricate periodontal tissues in the constrained oral cavity.[9]

Ultrasound elastography is an established method that facilitates the estimation of tissue mechanical properties by applying either a push force or by launching a low frequency wave into the biological tissue sites of interest. Tissue stiffness changes with pathology, and has thus been used to screen and diagnose diseases such as liver fibrosis, bowel disease, soft tissue tumors and malignancies, muscle spasm, and cardiovascular diseases.[10–12] In recent years, with the advent of speckle-tracking algorithms, quantitative strain, and strain velocity imaging have emerged as indispensable tools in the medical fields.[13] For the first time, we analyzed the strain of oral soft tissues with ultrasound imaging in vivo. Knowing the distinct strain differences between AM and G in the literature, we aimed to evaluate the feasibility of this newly developed ultrasound-based strain method to differentiate AM and G.

Materials and Methods

Two arms were involved in this study. A benchtop calibration study was conducted to determine the force which can be achieved for subsequent in vivo soft tissue strain. A preclinical pig study was conducted to observe and record soft tissue responses to externally induced stress.

Gel Pad Strain Calibration

A commercially available high-frequency linear array transducer (L30-8, Mindray Innovation Center NA, CA, USA) was used in this study to record periodontal regions of interest using a ZS3 cart-style ultrasound scanner (Mindray Innovation Center NA, CA, USA). The transducer was operated in tissue harmonic mode with a transmit frequency of 12 MHz and received at 24 MHz to suppress clutter from adjacent hard tissue surfaces. Spatial compounding was enabled with 3 steer angles to enhance the delineation of in-plane curved tissue interfaces. Due to an elevational focus of 8 mm, a standoff gel pad

(Aquaflex Ultrasound Gel Pad, Parker Laboratories, NJ, USA) was employed to reduce the risk of losing ultrasound gel when holding the aperture side-ways (Figure 1).

The gel pad was customized to fit the study's specific needs. A nominal size of 15 mm (L) by 5 mm (W) by 5 mm (T) was cut using a standard scalpel with disposable blades. An additional size was cut with a thickness (T) of 6 mm, to observe any potential changes due to thickness variations. We secured the standoff on the transducer as described previously.[14]

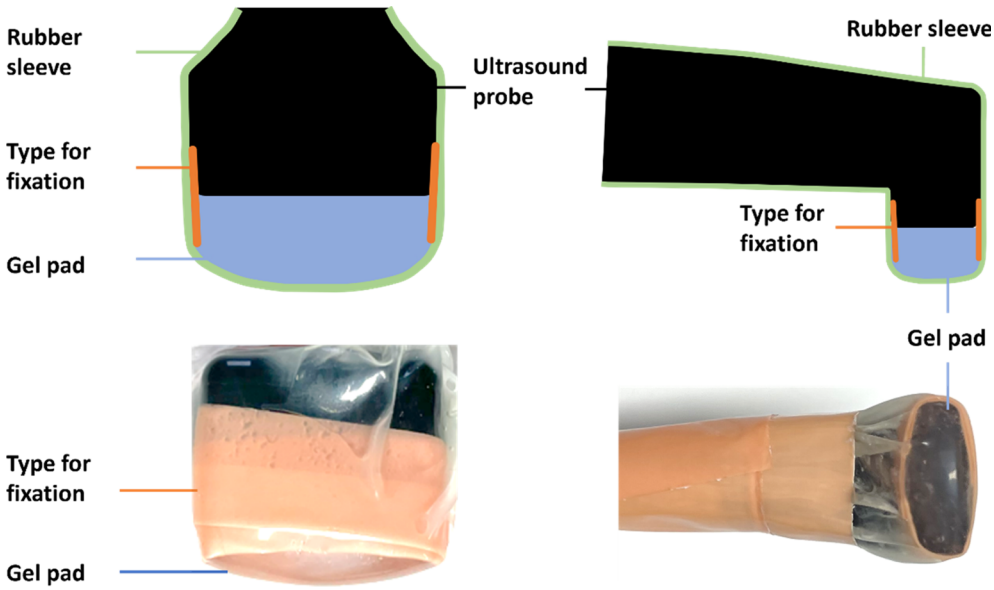
Figure 2 shows the general setup used to calibrate the stress–strain response of the standoff gel pad. The transducer was mounted on a linear motion stage that allowed for sub-millimeter-controlled vertical displacements. To induce stress, we pushed the gel block against the surface of a standard laboratory mass scale with a display for mass and force (Ohaus CS 2000, Ohaus Corporation, USA). Sandwiched between the transducer aperture and the scale's surface, we were able to image and quantify the gel block thickness in B-mode.

Concurrently we could read the force that the standoff would produce onto the scale as a result of the induced stress. The scale was zeroed after placing 3 g of coupling gel. A range of 0 to 250 g was recorded with an increment of 5 g up to 50 g and an increment of 50 g beyond that. Experimental variation was assessed by testing 3 samples for both thicknesses. Gel pad thickness was measured using 3D Slicer, a public-domain medical imaging software (version 5.0.3, National Alliance for Medical Image Computing).[15,16] The resulting force and strain data pairs were tabulated in Microsoft Excel (Microsoft Corp., Redmond, WA, USA) and further processed using custom Matlab scripts.

Preclinical Model

Sinclair mini pigs (n = 10) were used as a preclinical model for periodontal ultrasonography. The study was conducted at the University of Michigan, Medical School, with guidance and after protocol approval by the Institutional Animal Care & Use Committee (IACUC, Approval number: PRO00010333). No informed consent was needed, as no human subjects were involved. Six female and 4 male pigs with ages between 6 and 18 months were obtained and after 1 week of acclimatization, their teeth were prepared by standard oral prophylaxis (teeth cleaning).

Figure 1. Illustration of the preparation of the employed ultrasound transducer. The linear array has a sideways aperture with an elevational focus of 8 mm. A standoff gel pad is placed onto the transducer under fixation of a surrounding tape, and both are covered by a disposable rubber sleeve.



Ultrasound scans were performed after 1 additional week of housing. All pigs were imaged while under general anesthesia of 3% isoflurane administered through an endotracheal tube. Breathing was stabilized by a mechanical ventilator to 13 to 15 cycles per minute according to blood oxygenation and exhaled carbon dioxide. Additional vital monitoring included heart rate and core body temperature.

Figure 2. Setup used to provide a controlled mechanical deformation of the standoff gel pad. Left: The induced stress is quantified in Newtons by the scale upon which the standoff rests. Concurrently the resulting strain of the gel block was assessed from the B-mode image shown on the right.

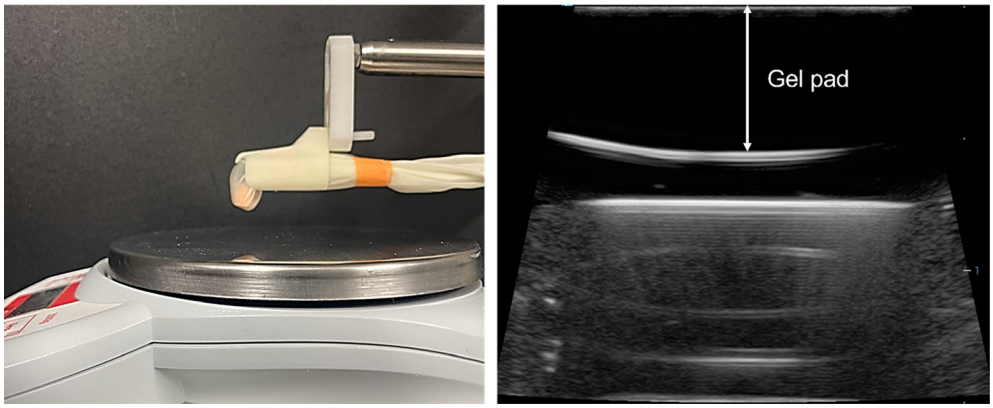
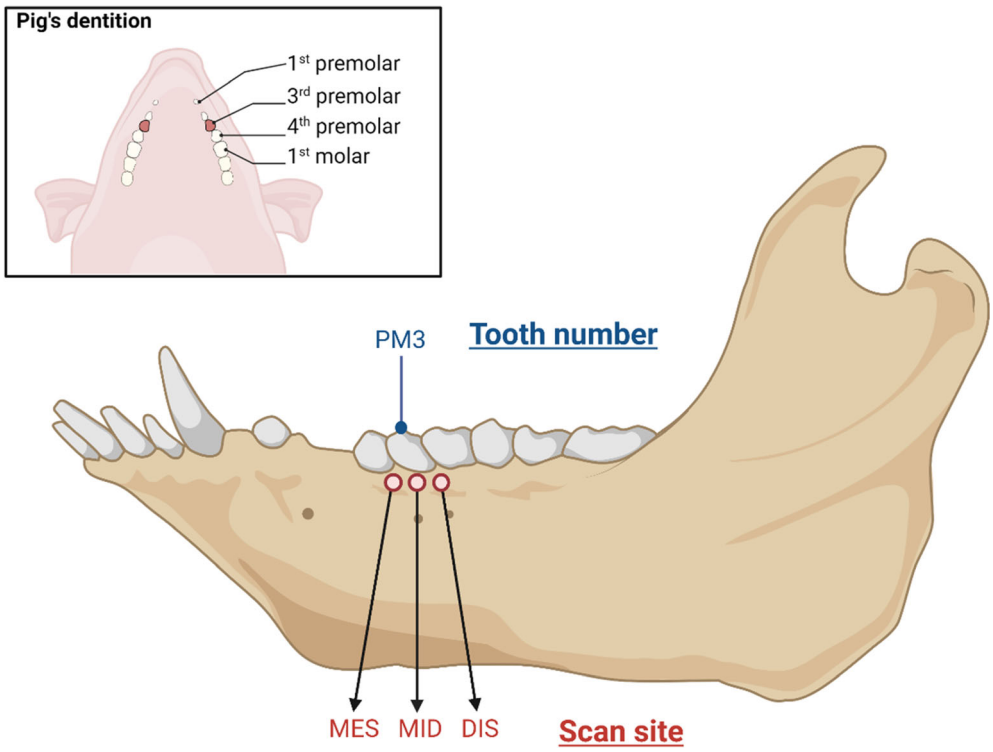


Figure 3. Anatomical illustration of the oral regions of interest. For this study, third premolars of all 4 quadrants were scanned. Sagittal midfacial, as well as mesial and distal interproximal sites were acquired. Created with BioRender.com.



Maxillary and mandibular permanent third premolars were included in this study.

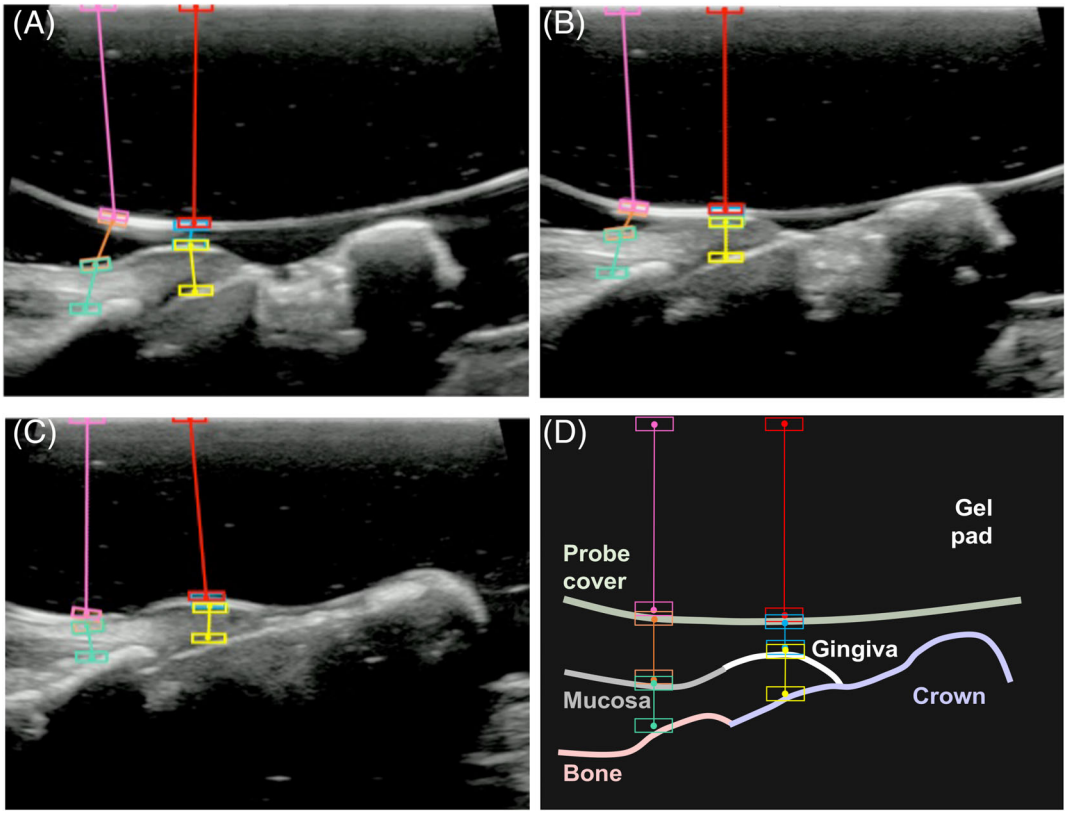
Oral Mucosa Ultrasonography

All scans were obtained along the buccolingual direction of the third premolar tooth (PM3) mid-facial (MID), mesial interdental area (MES), and distal interdental area (DIS) of both maxilla and mandible (Figure 3). The probe was centered on the marginal gingiva and a push was applied toward the soft tissue until the gel pad experienced a strain of more than 30% (see Figure 4). This sequence was recorded using the cine-loop function of the ultrasound scanner. It must be noted that preceding this sequence, an adequate amount of coupling gel (free gel) was applied between the imaging site and the transducer. Also, the operator always maintained this layer of free gel before the cine-loop recording was started. Otherwise, the soft tissue might have already been under a nonzero stress.

Strain Analysis

All cine-loop videos were imported into a processing engine for speckle-tracking strain analysis (EchoInsight®, V3.2.4.8100, Epsilon Imaging Inc, Ann Arbor, MI, USA). There, groups of regions of interest (ROIs) were created and placed in both, the gingival and the alveolar mucosal region. Figure 4 illustrates this process. To determine the longitudinal strain of the gingiva (yellow line in Figure 4), its initial thickness $l_G(0)$ was recorded as well as the

Figure 4. Illustration of the employed strain analysis of oral soft tissues. Shown here is the assessment of longitudinal (compressional) strain. **A**, B-mode showing a mid-facial sagittal view plane (consult panel **D** for tissue and other annotations). Note that the probe cover does not touch gingiva nor alveolar mucosa, that is, we expect no pressure from the gel pad on these tissues. Panels **B** and **C** show how subsequently a mechanical push onto these tissues was executed. Speckle tracking facilitated the assessment of the spatial dimensions during the push. For each site (yellow-gingiva and green-alveolar mucosa) 3 box-pairs were placed to assess strain in (1) the gel pad (red and magenta), (2) the free coupling gel (blue and orange) between the probe cover and tissue, and (3) the tissue strain (yellow and green). Strain data was obtained for the entire cine-loop of the actual push.



thickness in each frame of the cine-loop $l_G(N)$, to then obtain.

$$\varepsilon_G(N) = \frac{l_G(\mathrm{N}) - l_G(0)}{l_G(0)} \quad (1)$$

The strain of the standoff gel pad (red) is obtained as this part of the standoff is stressing the gingiva:

$$\varepsilon_S(N) = \frac{l_S(\mathrm{N}) - l_S(0)}{l_S(0)} \quad (2)$$

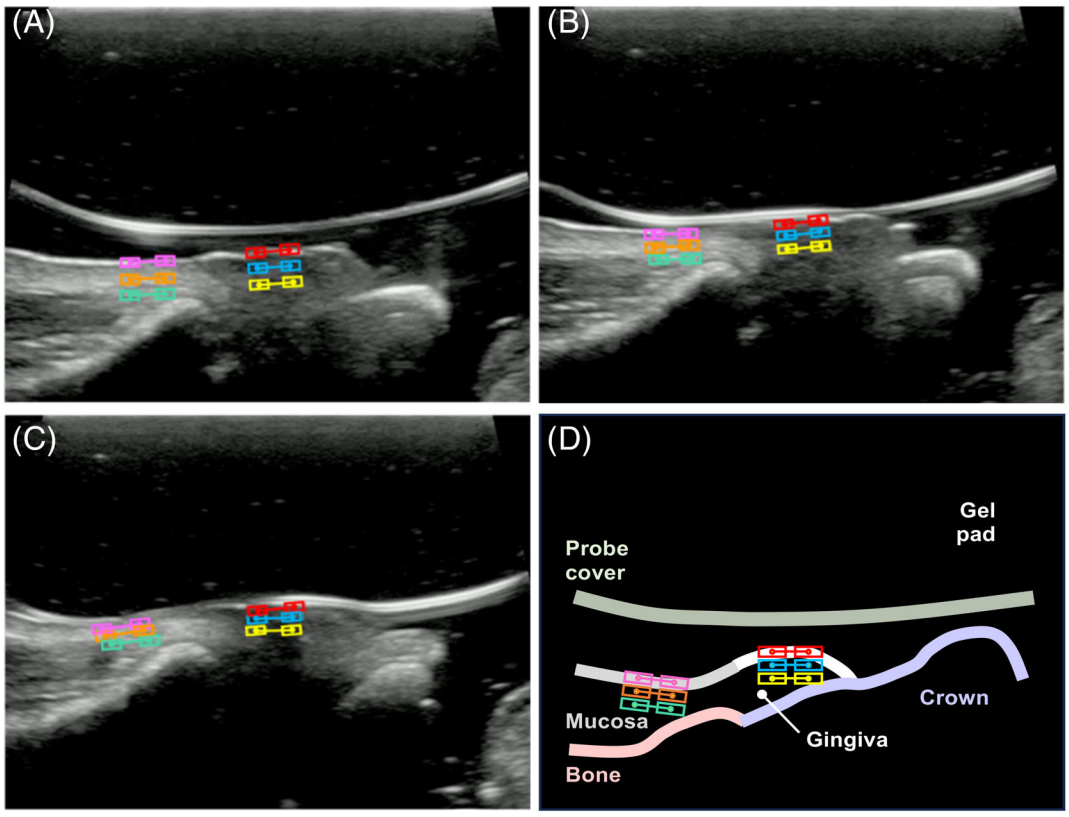
In addition, the strain of the free gel (blue) in-between the soft tissue and the transducer was recorded as:

$$\varepsilon_F(N) = \frac{l_F(\mathrm{N}) - l_F(0)}{l_F(0)} \quad (3)$$

Analogous to this longitudinal strain of the alveolar mucosa ε_{AM} was found for each frame as $\varepsilon_{AM}(N)$, as well as those for the associate free gel and the standoff pad.

Longitudinal strain speckle tracking boxes were placed either at interfaces or hard boundaries. During a push with finite stress from the gel pad, all free gel was displaced. During that time one speckle tracking box of the standoff pad was on the transducer aperture and the other on the gingival epithelial surface. One box of the gingival box-pair was also on the gingival epithelial surface and the other on the tooth surface.

Figure 5. Analogous to Figure 4, an example case with annotations for strain analysis. Here, however, the tensile stain is obtained. **A**, **B**, and **C** images: B-mode image with pairs of speckle tracking anchors for the assessment of tissue spreading during a mechanical push. Three box pairs are shown for the gingiva. The red box-pair resides on the epithelial surface of the gingiva. The blue box pair is placed 500 μm below the epithelial surface and the yellow pair is 1000 μm below the surface. The distance of the boxes within each pair was recorded for each push. In addition, the free gel and standoff gel pad strains were obtained from the estimate in Figure 4. The same scenario is also shown as an illustration in the **D** panel.



The tensile strain was estimated in a similar fashion. Figure 5 shows the placement of box pairs in the gingiva and alveolar mucosa which were tracking the stretching of tissue under the compressional stress of the standoff gel pad. The initial distance between 2 ROI boxes is set to 1000 μm. Three box pairs were placed, on, 500 μm below, and 1000 μm below the epithelial surface. All strain data were exported and analyzed using custom software (The Mathworks Inc, Natick, MA, USA).

Young's Modulus

Young's modulus was computed as

$$E = \frac{\sigma}{\varepsilon} \tag{4}$$

where $\sigma = \frac{F}{A}$ is the stress induced by the force F induced on the surface A. From the nominal surface area of the standoff pad, we compute A to 40 mm^2, whereas F is derived from the observed strain in the gel pad as described above. Strain ϵ given by Equation 1 as either ε_G or ε_M. Data was averaged across animals and quadrants. The mean Young's modulus E was computed from the averaged stress and averaged strain. To obtain the uncertainty of E was derived by propagation of uncertainty (propagation of error). E is the gradient of the ratio of σ and ε, thus

$$E = \sigma(\varepsilon) \tag{5}$$

$$\frac{\partial E}{\partial \varepsilon} = \frac{\partial \sigma(\varepsilon)}{\partial \varepsilon} = \frac{-\sigma(\varepsilon)}{\varepsilon^2} \tag{6}$$

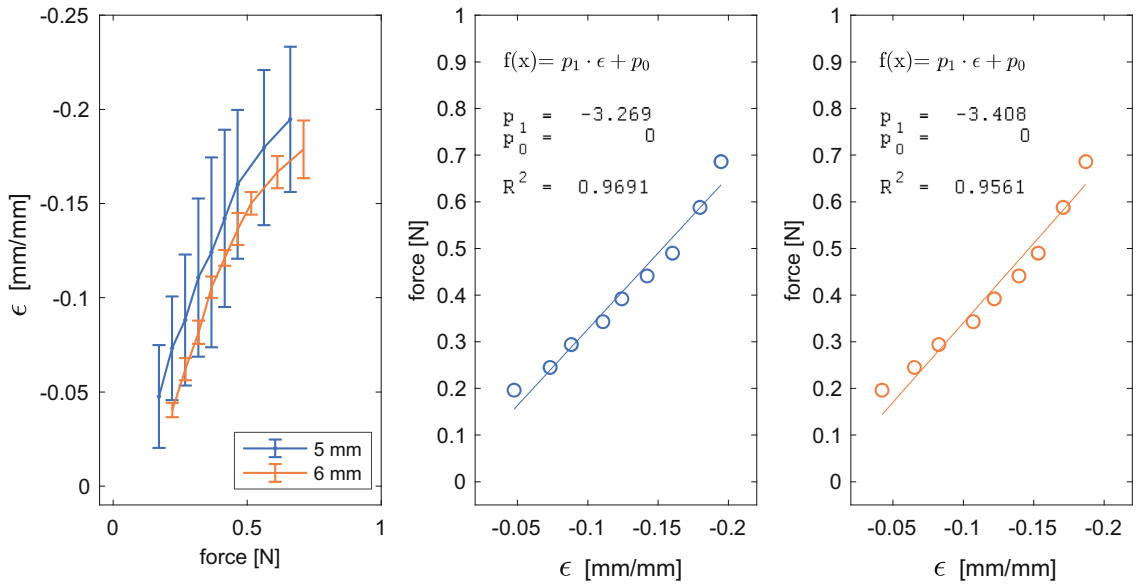
$$\partial E = \frac{\partial \sigma(\varepsilon)}{\partial \varepsilon} \partial \varepsilon = -E \frac{\partial \varepsilon}{\varepsilon} \tag{7}$$

For calibration purposes, a benchtop elastometer device (MicroElastometer, Model 0301, Artann Laboratories, West Trenton, NJ, USA) was employed to compare Young's modulus data obtained from our in vivo strain approach with that yielded by the elastometer. Sorbothane (Sorbothane Inc, Kent, OH, USA) a polyurethane based viscoelastic material was evaluated using the elastometer device as well as the above strain analysis.

Statistical Analyses

All longitudinal and tensile strain as well as force variables are expressed as mean and standard deviation. A 2-tailed *t*-test was used to examine the difference between groups of elasticity values. A *P*-value <.05 was considered to indicate a statistically significant

Figure 6. Gel pad strain calibration. Left: Average strain with a standard deviation of 3 estimates for 2 cases (5- and 6-mm gel pad thickness) as a function of applied force. Right: Inverted datasets with first order polynomial fit function, with $f(0) = 0$ constrain, for in vivo analysis.



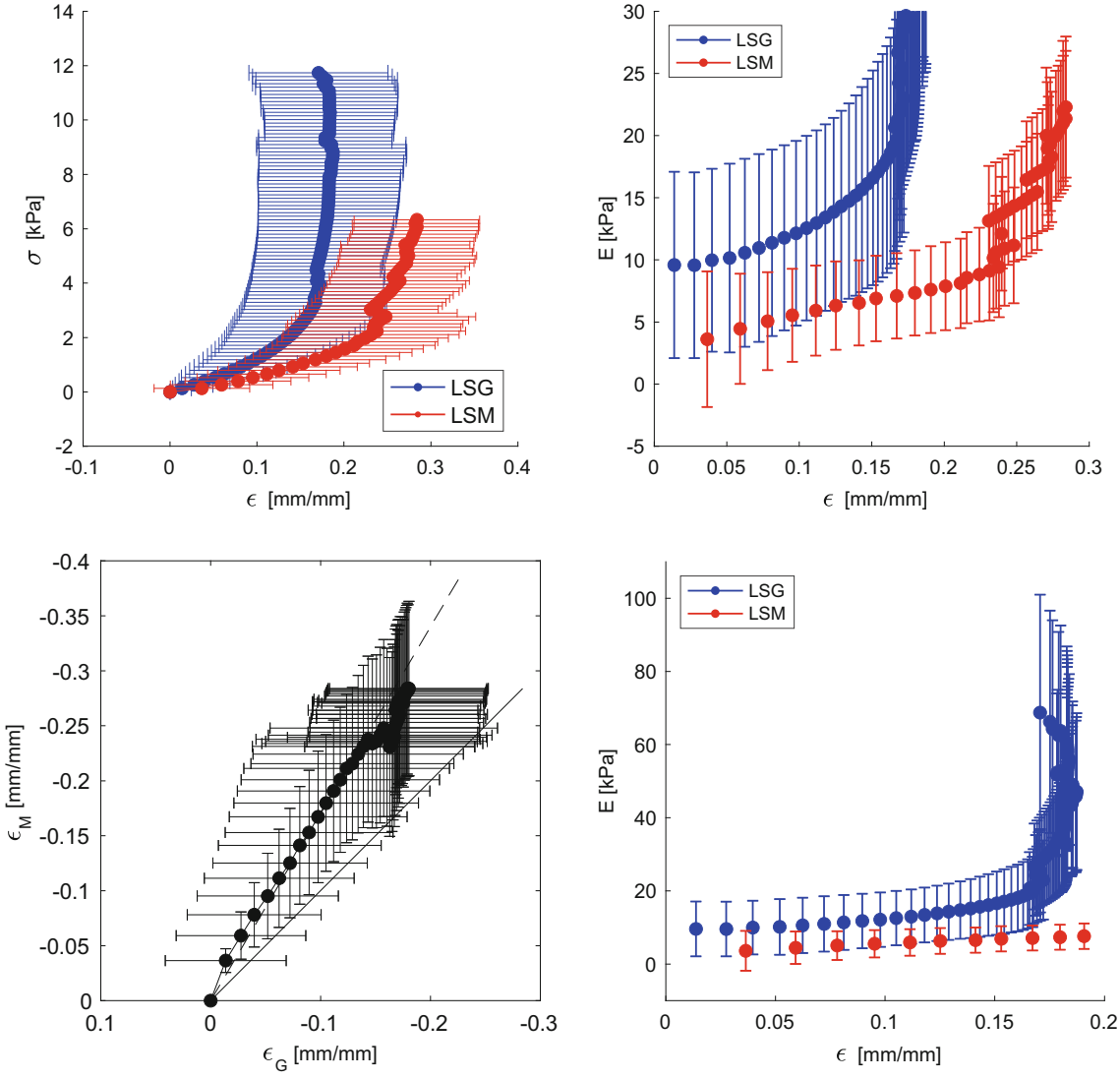
difference. Statistical analysis was performed using custom Matlab scripts.

Results

Gel Pad Strain Calibration

Figure 6 shows the obtained strain curve of the stand-off gel pad as a function of the applied force. Up to 2.45 N was applied to cover enough dynamic range for comparison to in vivo. Results are shown for both pad thicknesses. Each was measured 3 times and the mean is shown with standard deviation error bars. Using a measured gel pad surface area of $\sim$40 mm^2, the resulting testing compression pressure ranges from 0 to 25 kPa. The compressional strain of -0.195 ± 0.039 and -0.179 ± 0.015, was observed at 0.66 and 0.71 N, for the initial 5 and 6 mm thick

Figure 7. Longitudinal stress/strain analysis of gingiva (LSG) and alveolar mucosal (LSM) tissue. Left/top: Longitudinal stress (σ) versus strain (ε). Horizontal error bars indicate 1 standard deviation of the strain measurement. Top/right: Young's Modulus versus strain. Vertical error bars indicate 1 standard deviation of the underlying strain and include propagation of uncertainty using Equation 7. Alveolar mucosa varies from 4 to 7 kPa. When reaching -25% strain the modulus rapidly increases to 20 kPa. The gingiva starts at 10 kPa and increases to 15 kPa at -15% strain, where it rapidly increases to 50 kPa (bottom/right). Bottom/left: Mucosal ε_M versus gingival ε_G strain. Note that the resulting curve is mostly linear with $\varepsilon_{AM} \sim 1.7 \times \varepsilon_G$, as shown by the dashed line, which is at $\varepsilon_{AM} = 1.7 \times \varepsilon_G$, whereas the bisector is shown as a solid line.



gel pad, respectively. To obtain in vivo compression pressures, the calibration data was inverted (middle and right panel in Figure 6) and fitted using a first order polynomial with $f(0) = 0$ constrain to average negative strains up to 0.2. The resulting force-strain coefficients for the 5- and 6-mm initial gel pad thicknesses were $y = -3.269x + 0$ $(R^2 = 0.9691)$ and $y = -3.408x + 0$ $(R^2 = 0.9561)$, respectively. The elastometer yielded a value of 183 ± 6.4 kPa, for a 5 mm thick Sorbothane sample. The same sample was evaluated using the gel pad strain reference method, which yielded a Young's modulus of 180.1 ± 45.6 kPa.

Longitudinal Strain

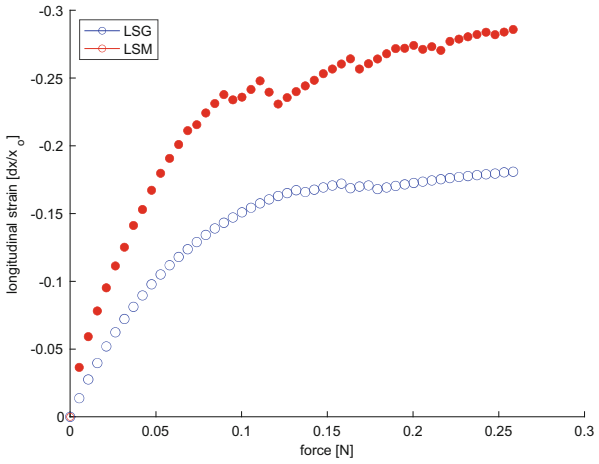
Alveolar mucosal and gingival longitudinal strain curves showed similar responses as a function of force. However, alveolar mucosal strain is significantly larger than gingival strain. Across the measured force range, $\varepsilon^L_{AM} \sim 1.7 \times \varepsilon^L_G$ as seen in the lower right panel of Figure 7. Comparing paired strain data of gingiva and alveolar mucosa for a fixed force, with *t*-test, yields significant differences (P value <.05) for all data points except for zero force (Figure 8).

Tensile Strain

The tensile strain pairs shown in Figure 5 at depths of 0, 0.5, and 1 mm from the gingival surface are subsequently labeled as TSG1, TSG2, and TSG3, respectively. Figure 9 shows the tensile strains TSG1 and TSM1. For a maximum stress of 11.7 kPa, the resulting strain TSG1 is 9.9%, whereas for a stress of 6.3 kPa the strain TSM1 is 20.6%, at which TSG1 is 7.5%. On average TSM1 ≈ 2 × TSG1. Tensile measurement results at 500 and 1000 µm depth are shown in Figures 10 and 11. Alveolar mucosa retains a strain of >10% at depth, whereas gingiva demonstrates an almost complete loss in tensile strain from an original 6%. As a consequence, the mixed plot of TSMn versus TSGn for n progressing from 1 to 3 (in Figures 9–11), shows a progressively steeper slope as the gingival strain diminishes.

Statistical differences between TSG1/TSM1 were found for forces larger than 0.08 N (Figure 12). The differences between TSG2 and TSM2 and TSG3 and TSM3 became more prominent, primarily due to the diminishing strain of the gingiva despite the increasing force. The differences were statistically significant for finite forces for both, 500 µm and 1000 µm depth. Within the same tissue, the strain in gingiva was significantly different among the 3 measuring depths, indicating a depth-dependent behavior, whereas in alveolar mucosa the strain was statistically different between TSM2 and TSM3 but not between TSM1 and TSM2 (Figure 13).

Figure 8. Statistical comparison of longitudinal strain of gingiva (LSG, blue) versus alveolar mucosa (LSM, red). Solid LSM circles are statistically different from the blue (LSG) counterparts at equal force. All LSM data is significantly different, except at zero force.



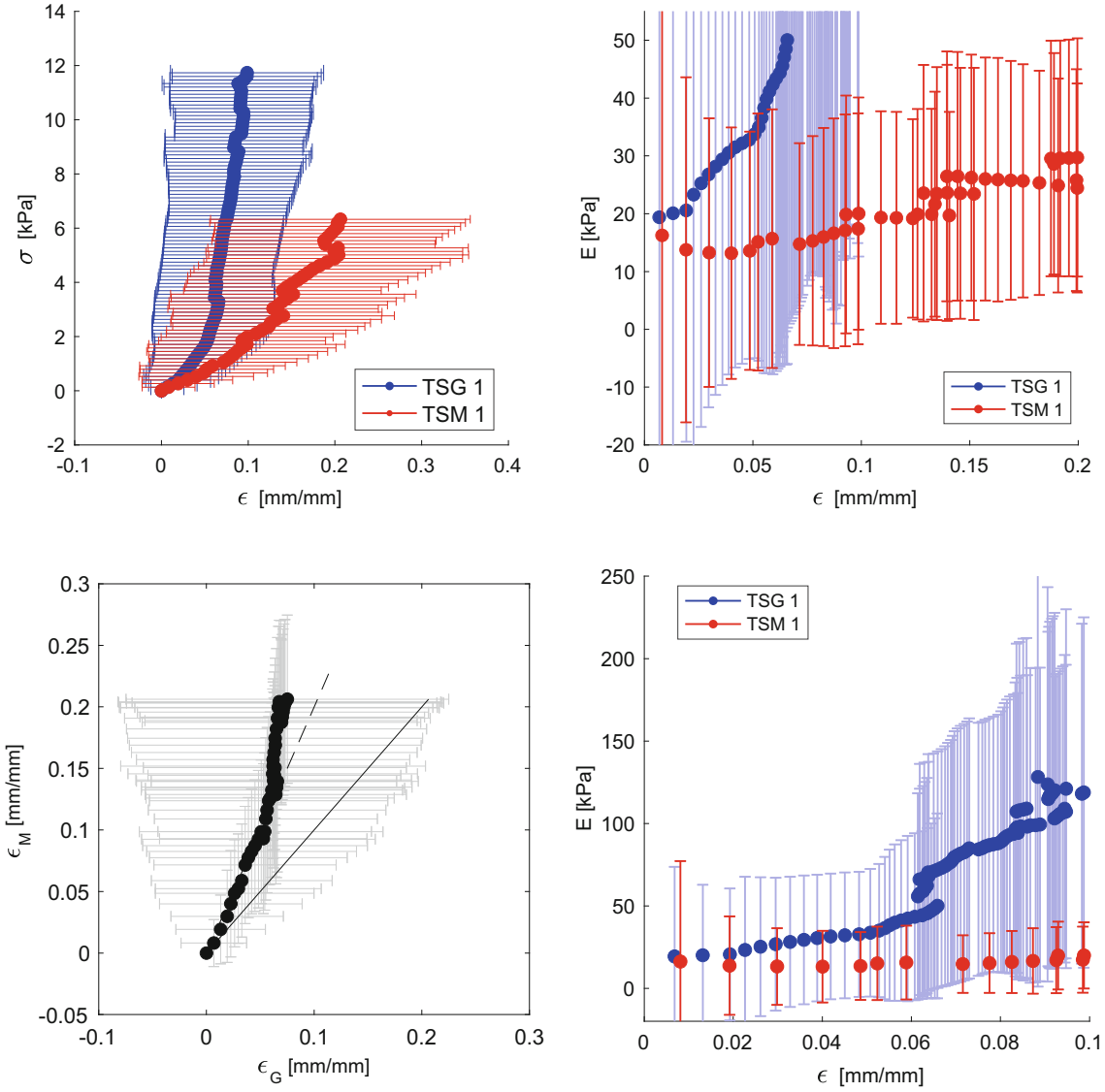
Discussion

In our study, we demonstrate that it is feasible to analyze oral mucosal tissue elasticity in vivo using high-frequency ultrasound. The 2 tested oral tissues, alveolar mucosa and gingiva showed distinct longitudinal and tensile strain values, although the behavior is similar. In Goktas's ex vivo study using porcine oral mucosa tissues, buccal attached gingiva exhibited a tensile strength of 3.94 ± 1.19 MPa, whereas buccal alveolar mucosa had a tensile strength of 1.29 ± 0.19 MPa, that is, 1/3 of that of gingiva.[6] A direct comparison of the results to our study was not possible because the contact area between the gel pad and soft tissue surface is difficult to define, which potentially flawed the Young's modulus calculation in our study. However, the calibration sample showed an excellent correspondence, with a difference of −1.6% or 2.9 kPa between calibration sample measurement and the reference elastometer. Nevertheless,

the current method can differentiate tissue elasticity between the gingiva and the alveolar mucosa. Tissue inflammation can increase interstitial fluid at the expense of collagen loss. These compositional changes can result in an alteration of tissue elasticity, thereby opening the door for quantitative evaluation of oral tissue inflammation, such as periodontitis.[17] Periodontitis affects more than 40% of the population, of age of 35 years and older, in the United States.[18] Therefore, once validated, this method may become a useful tool to quantify periodontal inflammation and inform treatment.

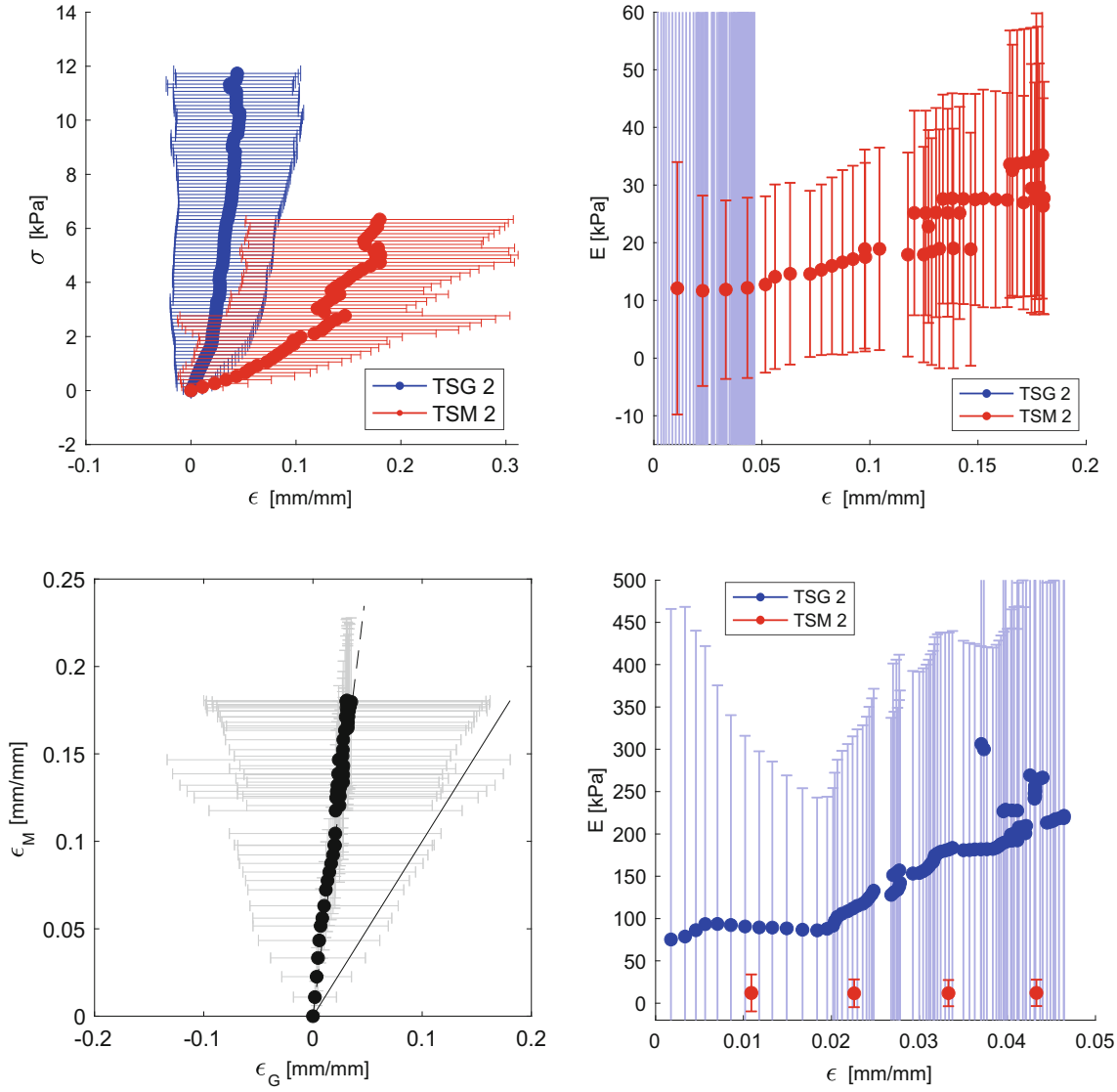
Oral mucosal tissues are sensitive to mechanical pressure and even small amounts of pressure

Figure 9. Tensile elastic properties of gingiva (TSG1) and alveolar mucosa (TSM1) both at the epithelial surface. Top/left: TSG1 and TSM1 stress (σ) as function of strain (ϵ), shown as mean and standard deviation error bars. Top/right: Tensile elastic modulus as a function of strain. Alveolar mucosa increases from 10 to 30 kPa. Gingiva shows a large increase from 20 to 120 kPa (see zoomed view on bottom/right). Bottom/left: TSM1 (ϵ_M) as a function of TSG1 (ϵ_G). Note that the resulting curve is mostly linear with $\epsilon_{AM} = \sim 2 \times \epsilon_G$, as indicated by the dashed line ($\epsilon_{AM} = 2 \times \epsilon_G$), while the bisector is shown as a solid line.



can induce a significant deformation.[1] Different types of oral epithelium showed similar responses as a function of force, that is, both exhibit viscoelastic properties.[11] Oral tissues exhibit a wide variety of biomechanical properties depending on their histological makeup, intracellular fluid content, and vascularity. While all mucosal tissues show viscoelasticity, some tissues are more elastic than others, and some more viscous. The viscoelasticity partially depends on the number of elastic elements such as actin, elastin, resilin, abductin, and collagen. Collagen is one of the most important elastic components of soft tissue. Different types of collagens provide different biomechanical behaviors.[19] Inflammation, edema, infection, tumors, or tissue necrosis, can induce cellular and

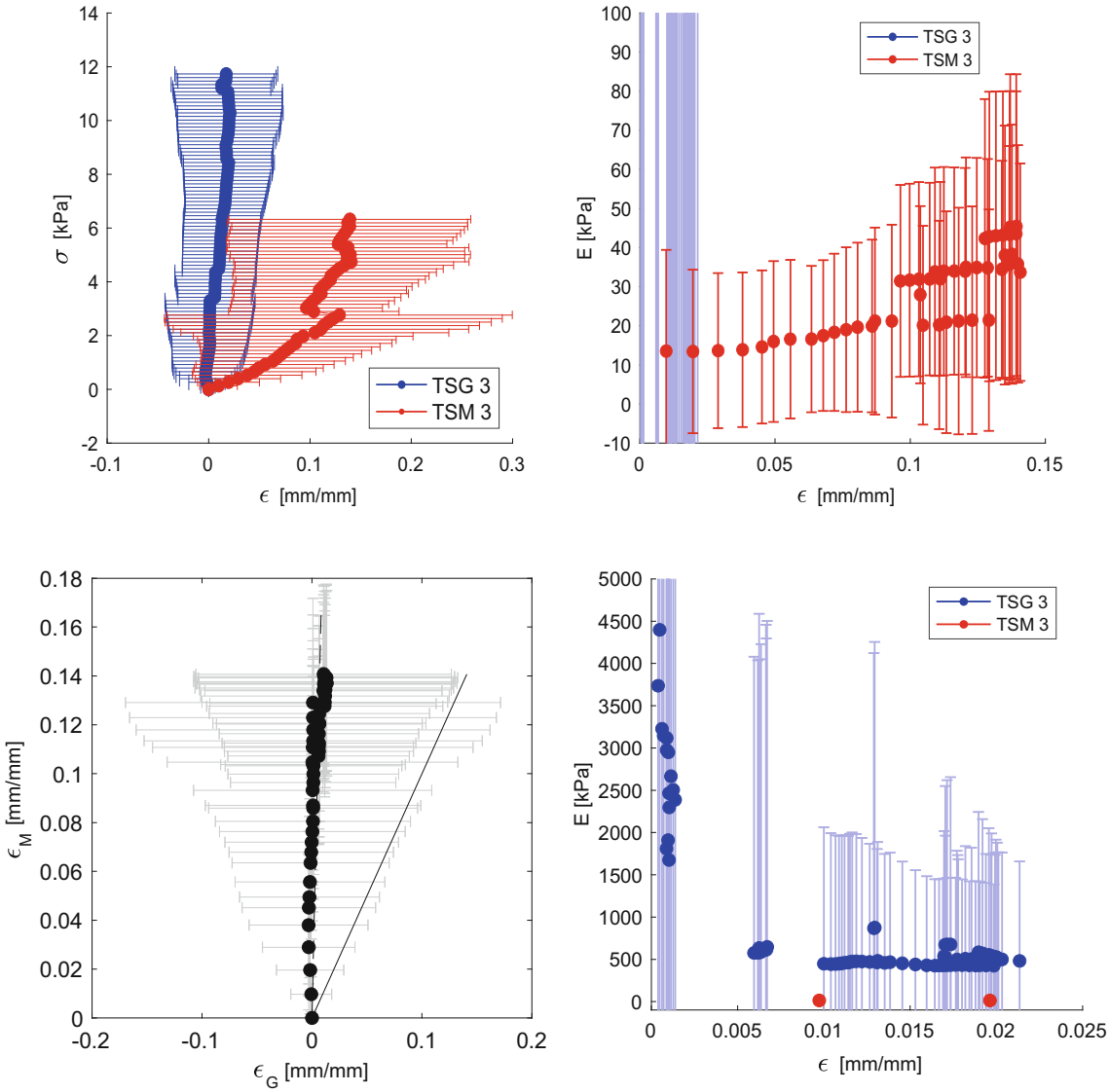
Figure 10. Tensile elastic properties of gingiva (TSG2) and mucosa (TSM2) at 500 μm below the epithelial surface. Top/left: TSG2 and TSM2 stress (σ) as function of strain (ε), shown as mean and standard deviation error bars. Top/right: Tensile elastic modulus as a function of strain. Alveolar mucosa hardens from ~10 to ~35 kPa. Gingiva hardens from 75 to 200 kPa (see zoomed view on bottom/right). Bottom/left: TSM2 (ε_M) as a function of TSG2 (ε_G). Note that the resulting curve is mostly linear with $\varepsilon_{AM} = \sim 5 \times \varepsilon_G$, as indicated by the dashed line ($\varepsilon_{AM} = 5 \times \varepsilon_G$), while the bisector is shown as a solid line.



extracellular responses that prompt changes in biomechanical properties.

Over the past century, numerous investigations have been conducted in an attempt to understand and quantify the mechanical properties of oral tissues. Several of them focused on the response of oral tissues to various types of mechanical loading.[6,20–23] Under mechanical loading, oral tissues undergo elastic deformation that can be measured through strain. Although these mechanical properties are keys to differentiating oral tissue types and diagnosing pathologies, literature regarding the in vivo testing of mechanical properties is scarce. This may be largely because the elastic modulus cannot be measured directly. In order to accurately

Figure 11. Tensile elastic properties of gingiva (TSG3) and mucosa (TSM3) at 1000 μm below the epithelial surface. Top/left: TSG3 and TSM3 stress (σ) as function of strain (ε), shown as mean and standard deviation error bars. Top/right: Tensile elastic modulus as a function of strain. Alveolar mucosa hardens from ∼15 to ∼40 kPa. Gingiva shows no consistent modulus until a strain of 1%, up on which a modulus of ∼500 kPa is observed (see zoomed view on bottom/right). Bottom/left: TSM3 (ε_M) as a function of TSG3 (ε_G). Note that the resulting curve is mostly vertical due to the nearly constant ε_M and the finite ε_G.The dashed line follows $\varepsilon_{AM} = 10 \times \varepsilon_G$, while the bisector is shown as a solid line.



quantify the elasticity of a tissue, an external mechanical pressure or a low-frequency wave (20–1000 Hz) need to be applied to induce deformation or internal vibrations within the tissue, while high-resolution imaging of internal tissue deformation must be performed, recorded, and analyzed for strain. If the target tissue is located near the surface, like skin, subcutaneous soft tissue, or muscle, external mechanical pressure can be easily applied. For deeper-seated organs in the body such as the liver, uterine, or intestine, acoustically induced waves can be used to obtain tissue elastic properties.[24]

Ultrasonography is a noninvasive, real-time, efficient, and accurate modality to acquire soft tissue images with high contrast. With the aid of special image analysis software (on the scanner or offline), it can also provide mechanical properties and functional parameters of living tissues. Strain and strain rate sonography has a pivotal role in echocardiography as well as ultrasonography of other organs such as liver, kidney, uterine, intestine, prostate, and others. There are several techniques to analyze the displacement of tissues: Visual inspection on M-mode or B-mode images,

Figure 12. Tensile strain of gingiva and alveolar mucosa at 3 depth levels. For each force value, a *P*-value is computed using *t*-test, to test for statistical significance between gingival and alveolar data. Red solid circles "●" indicate a significant difference between the tensile strain of mucosa compared to alveolar gingiva. TSM1 and TSG1 generally differ for forces greater than 0.08 N. TSM2 and TSG2 and TSM3 and TSG3 differ for finite forces, that is, greater than 0 N.

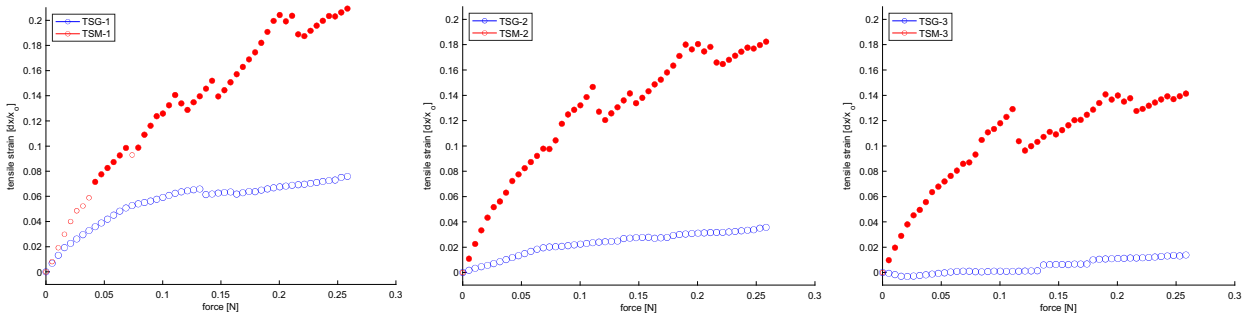
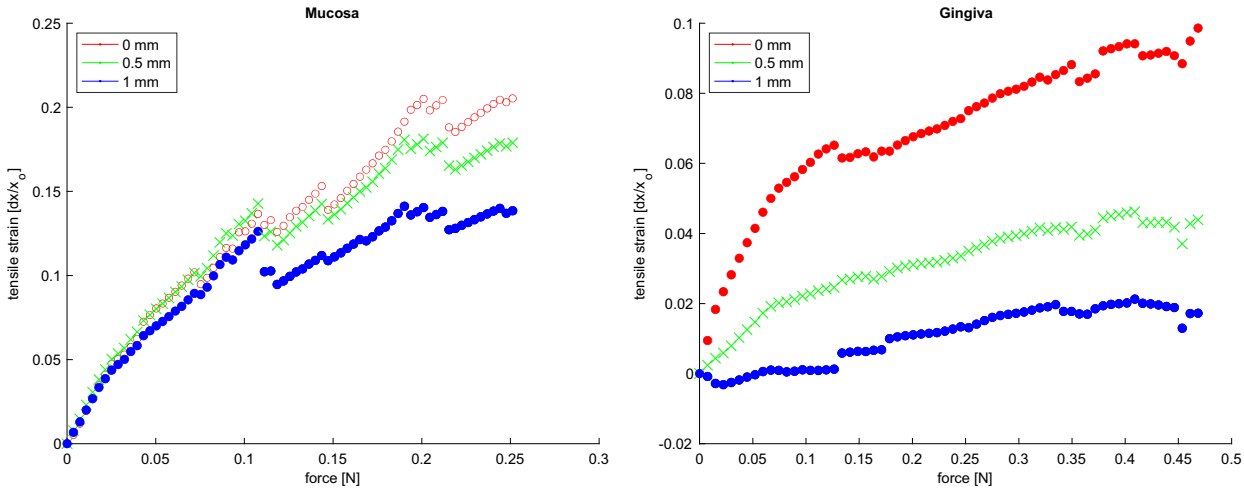


Figure 13. Comparison of tensile strain in gingiva and mucosa at 3 depth levels. Left: Alveolar mucosal tissue at 0, 500, and 1000 μm below the epithelium. Data points shown as green "X" are used as reference values. Red solid circles "●" indicate a significant difference between the tensile strain at the surface compared to 500 μm depth. Blue solid circles "●" indicate a significant difference between the tensile strain at 1000 μm depth compared to 500 μm depth. Hollow circles indicate no significant difference to the reference. Right: Same concept but for gingival tissue.



tissue velocity measurement, cross-correlation, and phase measurement techniques to quantify tissue displacement and strain.[25] In our study, the speckle tracking technique is used to analyze tissue displacement as a strain. The successful comparative assessment of gingiva and alveolar mucosa from this study warrants further research to quantify the biomechanical properties of other types of oral tissues in vivo at different conditions, for example, health and disease status. Moreover, standardization of the gel pad property and size could improve the accuracy of strain estimation in the future.

Conclusion

For the first time, the mechanical properties of 2 tissue types of porcine oral mucosa were contrasted in vivo with high-frequency ultrasound. Gingiva and alveolar mucosa both follow viscoelastic properties when subject to compressive force. A higher compressional, as well as tensile, modulus, is associated with gingiva, compared to alveolar mucosa. This noninvasive method, once further validated, could hold potential for quantitative evaluation of oral conditions and diseases, and their objective and quantitative monitoring.

Dental ultrasound is a safe, convenient, and noninvasive way to obtain detailed real-time images of both soft tissue and bone surface. Combined with strain elastography, dental ultrasound has the potential to become a valuable tool for clinical diagnosis, inflammation monitoring, wound healing prediction, and long-term follow-up.

Data Availability Statement

The data that support the findings of this study are available from the corresponding author upon reasonable request.

References

1. Kydd WL, Daly CH. The biologic and mechanical effects of stress on oral mucosa. *J Prosthet Dent* 1982; 47:317–329.
2. Squier CA, Kremer MJ. Biology of oral mucosa and esophagus. *J Natl Cancer Inst Monogr* 2001; 29:7–15.
3. Groeger S, Meyle J. Oral mucosal epithelial cells. *Front Immunol* 2019; 14:208.
4. Tsaira A, Karagiannidis P, Sidira M, et al. Theoretical considerations and a mathematical model for the analysis of the biomechanical response of human keratinized oral mucosa. *Front Physiol* 2016; 29:364.
5. Choi JJE, Zwirner J, Ramani RS, et al. Mechanical properties of human oral mucosa tissues are site dependent: a combined biomechanical, histological and ultrastructural approach. *Clin Exp Dent Res* 2020; 6:602–611.
6. Goktas S, Dmytryk JJ, McFetridge PS. Biomechanical behavior of oral soft tissues. *J Periodontol* 2011; 82:1178–1186.
7. Gasik M, Lambert F, Bacevic M. Biomechanical properties of bone and mucosa for design and application of dental implants. *Materials (Basel)* 2021; 14:2845.
8. Kaproth-Joslin KA, Nicola R, Dogra VS. The history of US: from bats and boats to the bedside and beyond: RSNA centennial article. *Radiographics* 2015; 35:960–970.
9. Chan HL, Kripfgans OD. *Dental Ultrasound in Periodontology and Implantology*. New York, NY: Springer; 2021.
10. Jiang J, Hall TJ. A generalized speckle tracking algorithm for ultrasonic strain imaging using dynamic programming. *Ultrasound Med Biol* 2009; 35:1863–1879.
11. Abu-Ata N, Dillman JR, Rubin JM, et al. Ultrasound shear wave elastography in pediatric stricturing small bowel Crohn disease: correlation with histology and second harmonic imaging microscopy. *Pediatr Radiol* 2023; 53:34–45.
12. Gao J, Rubin JM, Chen J, O'Dell M. Ultrasound elastography to assess botulinum toxin a treatment for post-stroke spasticity: a feasibility study. *Ultrasound Med Biol* 2019; 45:1094–1102.
13. Mirea O, Duchenne J, Voigt J. Recent advances in echocardiography: strain and strain rate imaging. *F1000Res* 2016; 5: F1000 Faculty Rev-787. https://doi.org/10.12688/f1000research.7228.1.
14. Kripfgans OD, Chan HL. Preliminary experience in transducer preparation for intraoral imaging. *J Ultrasound Med* 2023; 42:2155–2166.
15. 3D Slicer, version 5.0.3. https://www.slicer.org/. Accessed May 5, 2023.
16. Fedorov A, Beichel R, Kalpathy-Cramer J, et al. 3D slicer as an image computing platform for the quantitative imaging network. *Magn Reson Imaging* 2012; 30:1323–1341.
17. Kornman KS. Mapping the pathogenesis of periodontitis: a new look. *J Periodontol* 2008; 79:1560–1568.
18. Eke PI, Thornton-Evans GO, Wei L, Borgnakke WS, Dye BA, Genco RJ. Periodontitis in US adults: National Health and Nutrition Examination Survey 2009–2014. *J Am Dent Assoc* 2018; 149: 576–588.e6.
19. Fung YC. Bio-viscoelastic solids. In: Fung YC (ed). *Biomechanics*. New York, NY: Springer; 1981.
20. Ophir J, Alam SK, Garra BS, et al. Elastography: imaging the elastic properties of soft tissues with ultrasound. *J Med Ultrason* 2001; 29:155.

21. Komatsu K. Mechanical strength and viscoelastic response of the periodontal ligament in relation to structure. *J Dent Biomech* 2010; 2010:502318.
22. Inoue K, Arikawa H, Fujii K, Shinohara N, Kawahata N. Viscoelastic properties of oral soft tissue. *Dent Mater J* 1985; 4:47–53.
23. Krouskop TA, Dougherty DR, Vinson FS. A pulsed doppler ultrasonic system for making noninvasive measurements of the mechanical properties of soft tissue. *J Rehabil Res Dev* 1987; 24: 1–8.
24. Gao L, Parker KJ, Lerner RM, Levinson SF. Imaging of the elastic properties of tissue—a review. *Ultrasound Med Biol* 1996; 22:959–977.
25. Ophir J, Alam SK, Garra B, et al. Elastography: ultrasonic imaging of tissue strain and elastic modulus in vivo. *Proc Inst Mech Eng H* 1999; 213:203–233.